Supporting Information

Ambivalent binding between a radical-based pincer ligand and iron

Katie L. M. Harriman,[a,b] Alicea A. Leitch,[a,b] Sebastian A. Stoian,[c] Fatemah Habib,[a,b] Jared L. Kneebone,[d] Serge I. Gorelsky,[a,b] Ilia Korobkov,[a,b] Serge Desgreniers,[f] Michael L. Neidig,[d] Stephen Hill, [c,f] Muralee Murugesu,[a,b] and Jaclyn L. Brusso*[a,b]*

[a] Department of Chemistry and [b] Centre for Catalysis Research and Innovation, University of Ottawa, Ottawa, Ontario K1N 6N5, Canada.

[c] National High Magnetic Field Laboratory, Florida State University, Tallahassee, Florida 32306, USA.

[d] Department of Chemistry, University of Rochester, Rochester New York 14627, USA.

[e] Department of Physics, University of Ottawa, Ottawa, Ontario, K1N 6N5, Canada.

[f] Department of Physics, Florida State University, Tallahassee, Florida, 32306, USA.

*Corresponding Authors: J.L. Brusso (E-mail: jbrusso@uottawa.ca; Tel: +1 (613) 562 5800 ext 7091); M. Murugesu (E-mail: m.murugesu@uottawa.ca; Tel: +1 (613) 562 5800 ext 2733)

Contents

General Procedures and Starting Materials. The reagents 4-dimethylaminopyridine (Aldrich) and N-chlorosuccinimide (TCI America), ferric chloride (Sigma-Aldrich), and ferrous chloride (Alfa-Aesar) were obtained commercially and used as received unless otherwise stated. **Py_2TTAH** was prepared as outlined in the literature.[1] All solvents were of at least reagent grade; MeCN was dried by distillation from P_2O_5 and dimethylformamide (DMF) was dried over 4Å molecular sieves. All reactions were carried out in air unless otherwise stated. Infrared spectra were recorded on either a Cary 630 or Nicolet Nexus 550 FT-IR spectrometer using Attenuated Total Reflection in the 4000 – 600 cm^{-1} range. Resonance Raman spectra were obtained with an argon ion laser for 532 nm excitation, a Rayleigh scattering filter, and Peltier-cooled charge-coupled device (CCD) detector. Elemental analyses were carried out with a Costech EOS 4010 CHNSO analyzer. UV-visible spectra were measured using an Agilent Cary 5000 UV-Vis-NIR spectrophotometer in the range 200 – 1200 nm. Solution absorption measurements were completed on dichloromethane solutions with standard 10 mm pathlength cuvettes. Diffuse reflectance measurements were collected with the use of a Praying Mantis™ accessory by Harrick Scientific. Baseline correction was completed with Spectralon® reference.

Preparation of Py_2TTA. Under an inert atmosphere, **Py_2TTAH** (0.500 g, 1.96 mmol), 4-dimethylaminopyridine (0.136 g, 1.11 mmol) and N-chlorosuccinimide (0.134 g, 1.00 mmol) were combined and 5 mL degassed MeCN (3 freeze-pump-thaw cycles) was added, which afforded a maroon slurry. After 2h, the fine brown solid was filtered in vacuo and washed twice with 3 mL MeCN. Crude yield 0.175 g (0.688 mmol, 35%). Recrystallization from MeCN afforded black-brown microcrystalline material. IR: υ_{max} = 3050 (w), 3004 (w), 1641 (w), 1571 (w), 1530 (m), 1510 (m), 1489 (m), 1476 (m), 1461 (m), 1422 (m), 1396 (m), 1380 (s), 1345 (m), 1254 (m), 1231 (m), 1160 (w), 1112 (m), 1042 (w), 994 (m), 974 (w), 912 (w), 843 (w), 814 (w), 768 (s), 757 (m), 739 (s), 726 (s), 692 (m), 668 (w) cm^{-1}. Anal. Calcd for $C_{12}H_8N_5S$: C, 56.68; H, 3.17; N, 27.54. Found: C, 56.90; H, 3.37; N, 27.66.

Preparation of $Fe(Py_2TTA)Cl_2$ (1). *Route 1:* Under an inert atmosphere, a solution of ferrous chloride (0.252 mmol, 32 mg) in degassed MeCN (5 mL) was layered on top of a degassed solution of **$(Py_2TTA)_2$** (0.125 mmol, 32 mg) in $CHCl_3$ (5 mL). X-ray quality green-brown crystals grew from the reaction mixture after 3d. *Route 2:* A solution of ferric chloride (0.500 mmol, 82 mg) in MeOH (5 mL) was layered on top of a solution of **Py_2TTAH** (0.250 mmol, 64

mg) in DMF (5 mL). Green-brown block-like crystals suitable for X-ray diffraction grew from the reaction mixture after 3d. Yield = 82%. IR (neat, cm^{-1}): 1600, 1561, 1514, 1464, 1441, 1287, 1273, 1261, 1171, 1145, 1096, 1058, 1039, 1020, 967, 787, 764, 750, 743, 724, 671, 647, 638. Calcd for $C_{12}H_8Cl_2FeN_5S$: C, 37.82; H, 2.12; N, 18.38; S, 8.41. Found C, 37.87; H, 1.94; N, 18.28; S, 8.13.

Electrochemistry. Cyclic voltammetry was performed using a BASi Epsilon potentiostat employing a glass cell and platinum wires for working, counter and pseudo-reference electrodes. The measurements were carried out on dichloromethane solutions (dried by Innovative Technology PureSolv solvent system and stored over 4 Å molecular sieves) containing 0.1 M tetrabutylammonium hexafluorophosphate (Aldrich) as supporting electrolyte with a scan rate of 100 mV/s. The experiments were referenced to the Fc/Fc^+ redox couple of ferrocene at +0.48 V vs. SCE.[2]

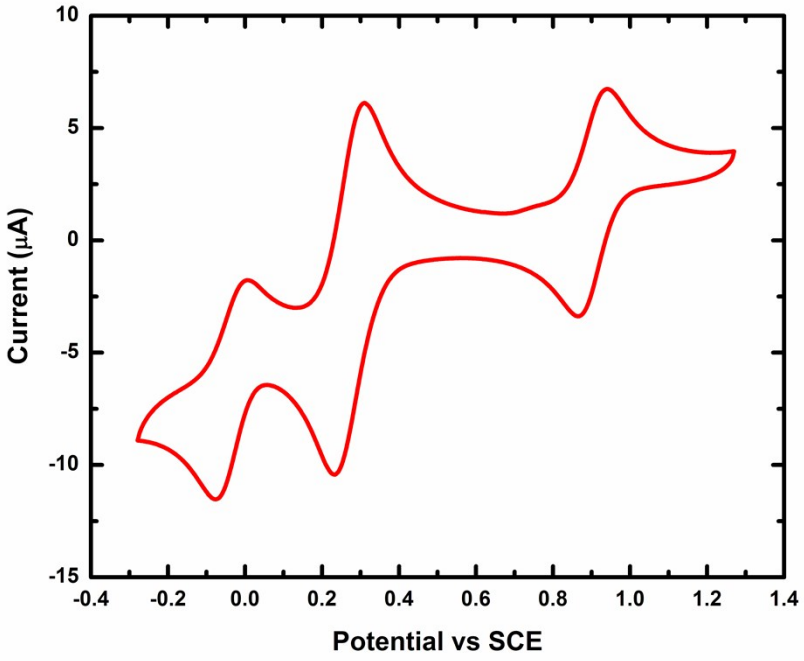

Figure S1 Cyclic voltammogram of **$Fe(Py_2TTAO)Cl_2$:$Fe(Py_2TTA)Cl_2$** (in ~1:1 ratio as determined by single crystal X-ray analysis; see Figure S2) in DCM solution (0.1M $[Bu_4N][PF_6]$, 100 mV s^{-1}).

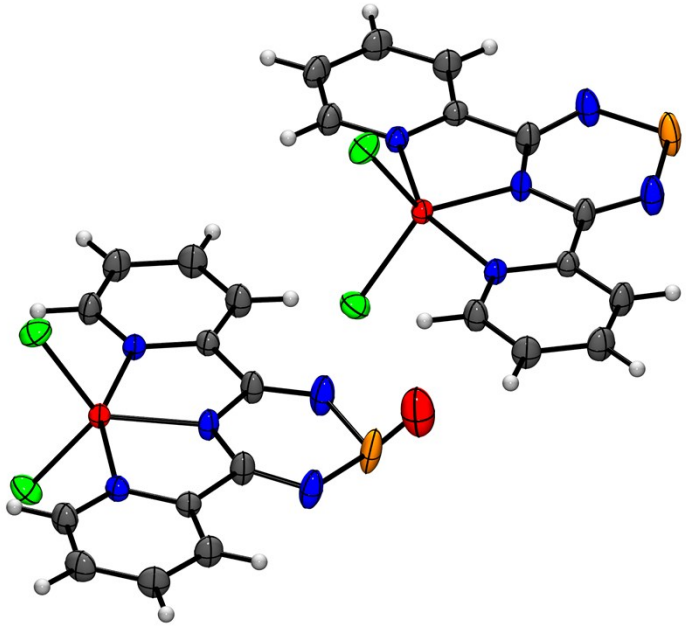

Figure S2. Molecular unit of **Fe(Py_2TTAO)Cl_2**:**Fe(Py_2TTA)Cl_2** in a 1:1 ratio.

Molar Absorptivity. To obtain the molar extinction coefficients, a series of dichloromethane solutions were prepared (concentrations in μM for **1**: 131/65/33/16/8; and **Py_2TTAH**: 196/98/49/24/12) and analyzed by UV-vis spectroscopy. The results of the studies are presented in Figure S3 and Table S1.

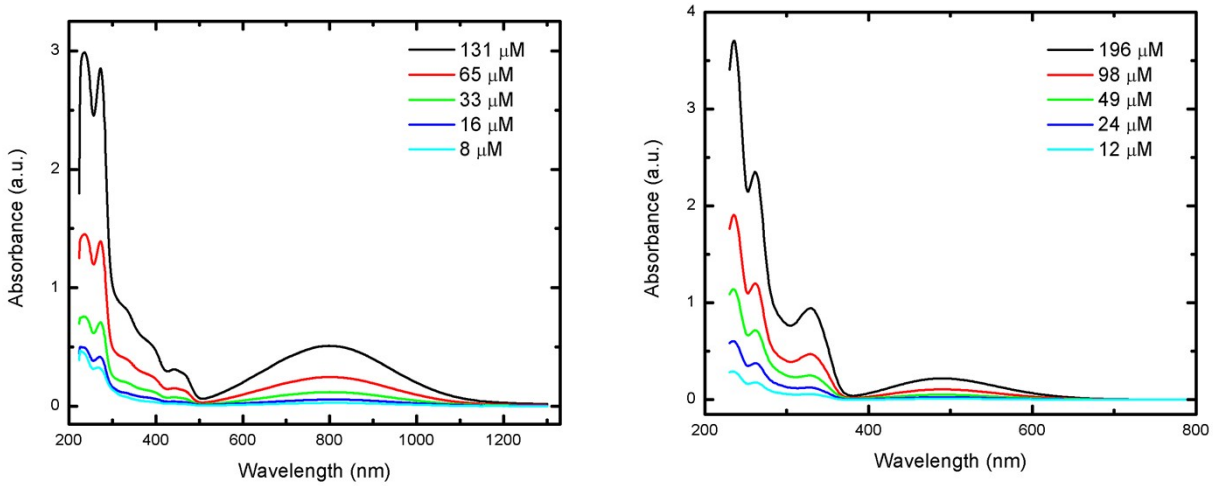

Figure S3. Solution emission spectra of **1** (left) and **Py_2TTAH** (right) in DCM.

Table S1. Molar extinction coefficients (in DCM) for complex **1** and **Py_2TTAH**.

1		**Py_2TTAH**	
λ (nm)	ε ($\mu M^{-1} cm^{-1}$)	λ (nm)	ε ($\mu M^{-1} cm^{-1}$)
235	0.0211	235	0.0182
272	0.0209	261	0.0116
800	0.00393	329	0.00479
–	–	489	0.00114

Crystal Growth. Crystals of **1** were grown from a mixture of MeOH/DMF at room temperature.

Single Crystal X-ray Diffraction Studies. Data collection results for **Fe(Py_2TTA)Cl_2** represent the best data sets obtained in several trials. The crystals were mounted on thin glass fibers using paraffin oil. Prior to data collection crystals were cooled to 200(2) K. Data were collected on a Bruker AXS KAPPA single crystal diffractometer equipped with a sealed Mo tube source (wavelength 0.71073 Å) APEX II CCD detector. Raw data collection and processing were performed with APEX II software package from BRUKER AXS.[5] Diffraction data for **Fe(Py_2TTA)Cl_2** were collected with a sequence of 0.3° ω scans at 0, 120, and 240° in φ. Initial unit cell parameters were determined from 60 data frames with 0.3° ω scan each, collected at the different sections of the Ewald sphere. Semi-empirical absorption corrections based on equivalent reflections were applied.[6] Systematic absences in the diffraction data-set and unit-cell parameters were consistent with orthorombic **P***nma* (№62) for **Fe(Py_2TTA)Cl_2**. Solutions in the centrosymmetric space groups for all samples yielded chemically reasonable and computationally stable results of refinement. Structures were solved by direct methods, completed with difference Fourier synthesis, and refined with full-matrix least-squares procedures based on F^2.

Results of refinement for **Fe(Py_2TTA)Cl_2** display one molecule of target compound located on mirror plane. Slight elongation of thermal ellipsoids for S(1), N(2) and N(3) atoms suggest non-planar arrangement of the ring. Within this arrangement sulfur and pair of nitrogen atoms are located on the opposite sides of the mirror plane with overall 50% : 50% disorder; however, refinement of such model demonstrates significant improvement of refinement figures.

All hydrogen atom positions were calculated based on the geometry of related non-hydrogen atoms and were treated as idealized contributions during the refinement. All scattering factors are contained in several versions of the SHELXTL program library, with the latest version used being v.6.12.[7] Crystallographic data and selected data collection parameters are reported in Table S1.

Table S2. Crystallographic data and selected data collection parameters.

Compound	**$Fe(Py_2TTA)Cl_2$**
Empirical formula	$C_{12}H_8Cl_2FeN_5S$
Formula weight	381.04
Crystal size, mm	0.20 x 0.16 x 0.14
Crystal system	Orthorhombic
Space group	**P***nma*
Z	4
a, Å	13.7473(4)
b, Å	7.1687(2)
c, Å	14.4831(3)
α, °	90
β, °	90
γ, °	90
Volume, $Å^3$	1427.31(6)
Calculated density, Mg/m^3	1.773
Absorption coefficient, mm^{-1}	1.575
T (K)	200(2)
F(000)	764
Θ range for data collection, °	2.04 to 28.30
Limiting indices	h = ±18, k = ±7, l = ±18
Reflections collected / unique	18203 / 1890
R(int)	0.0181
Completeness to Θ = 28.32, %	98.4
Max. and min. transmission	0.7457 and 0. 0.6753
Data / restraints / parameters	1890 / 0 / 124
Goodness-of-fit on F^2	1.066
Final R indices [I>2σ(I)]	R_1 = 0.0206, wR_2 = 0.0579
R indices (all data)	R_1 = 0.0218, wR_2 = 0.0590
Largest diff. peak/hole, $e \cdot Å^{-3}$	0.370 / -0.440

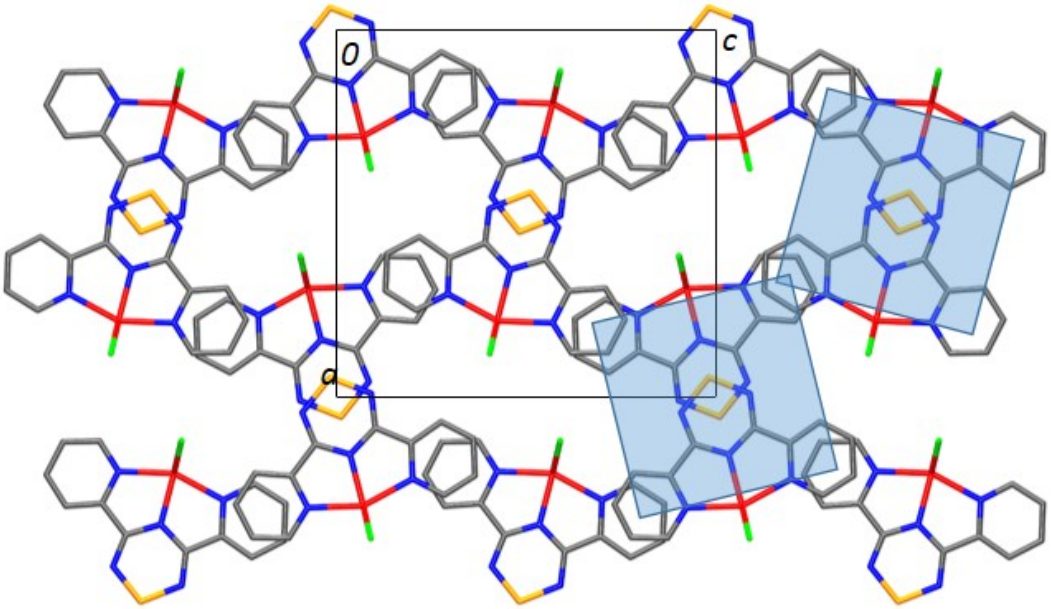

Figure S4. Crystal packing of **1** viewed along the *b*-axis.

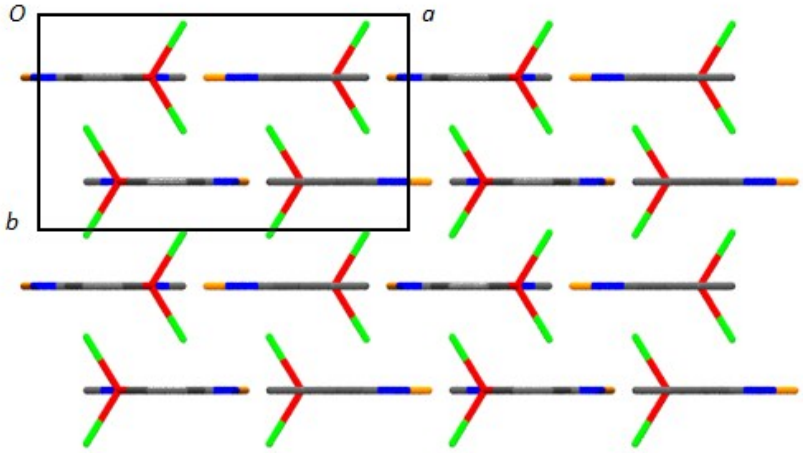

Figure S5. Layers of discrete molecules interacting in a head-to-tail fashion along the *a*-axis, which alternate along the *c*-axis.

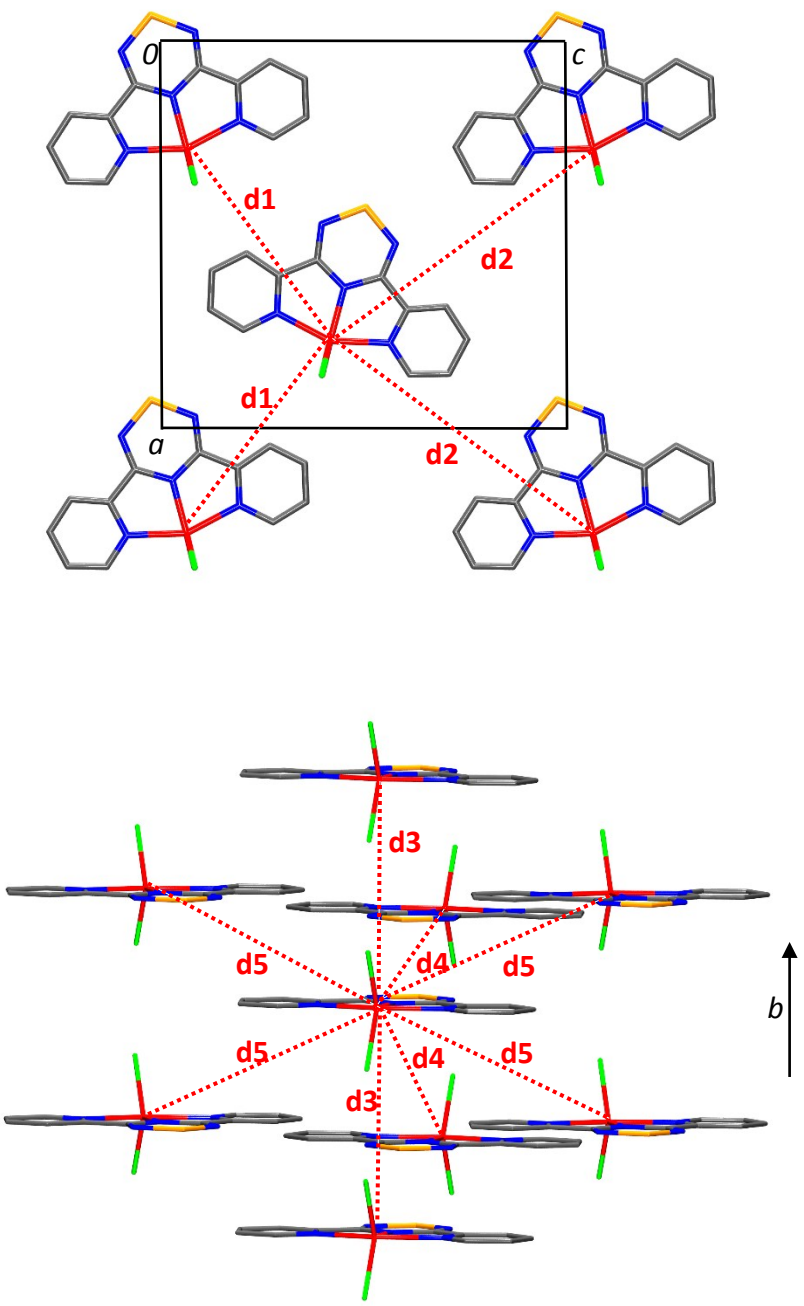

Figure S6. Fe-Fe' distances in the molecular plane (top) and above and below the molecular plane (bottom) in **1**. d1 = 8.57; d2 = 11.62; d3 = 7.17; d4 = 7.03; d5 = 8.17 Å

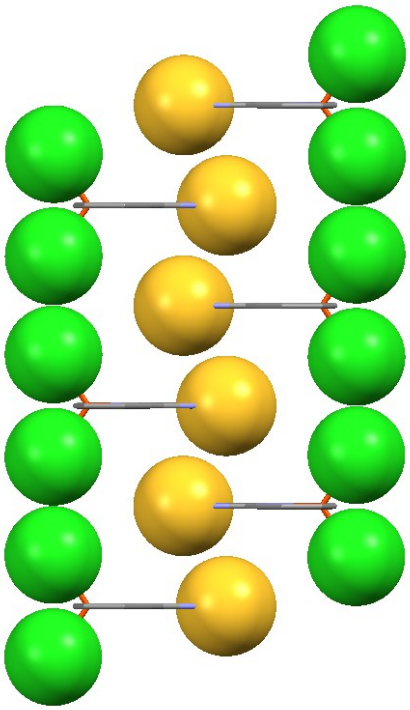

Figure S7. Packing diagram exhibiting a chain-like arrangement with space-filling view of the chloride ions (green) and sulfur atoms (yellow) in **Fe(Py_2TTA)Cl_2**. The close proximity of these atoms demonstrates the potential pathways for magnetic exchange.

Magnetic Measurements. The magnetic susceptibility measurements were obtained using a Quantum Design SQUID magnetometer MPMS-XL7 operating between 1.8 and 300 K. DC measurements were performed on a polycrystalline samples of 18.2 mg of **Fe(Py_2TTA)Cl_2**. Samples were wrapped in a polyethylene bag, and subjected to a field of 0 to 7 T. The magnetization data were collected at 100 K to check for ferromagnetic impurities that were absent in the sample. Diamagnetic corrections were applied for the sample holder and the inherent diamagnetism of the sample was estimated with the use of Pascals constants.

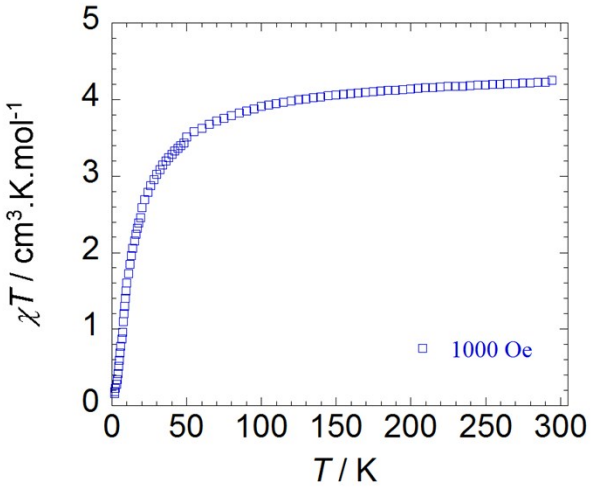

Figure S8. Temperature dependence of the χT at 1000 Oe for **Fe(Py$_2$TTA)Cl$_2$** (with χ being the molar susceptibility per complex defined as M/H).

^{57}Fe Mossbauer Spectroscopy. All samples characterized using ^{57}Fe Mössbauer spectroscopy consisted of non-enriched, as-isolated ground powder samples. The spectrum of Figure S9 was recorded in Rochester using a See Co. MS4 Mössbauer spectrometer integrated with a Janis SVT-400T He/N_2 cryostat for measurements at 80 K with a 0.07 T applied magnetic field. The absorber used for this spectrum was prepared in an inert atmosphere glove box equipped with a liquid nitrogen fill port to enable sample freezing to 77 K within the glove box. The sample was then loaded into a Delrin® Mössbauer sample cup and for measurements was loaded in the spectrometer under liquid nitrogen. All other ^{57}Fe Mössbauer spectra presented in this manuscript were recorded in Tallahassee at the Mössbauer facility of the EMR division of the NHFML. The absorbers used for recording these spectra were obtained by dispersing ~ 50 mg complex in Nujol® mineral oil contained in a polyethylene container. These spectra were collected using a spectrometer of a constant acceleration type that was fitted with a Janis 8DT Super Varitemp liquid helium cryostat and an 8 T superconducting magnet. This setup allowed for applying variable magnetic fields parallel to the incoming γ-radiation. The source consisted of 100 mCi ^{57}Co diffused in a rhodium foil and was incorporated in a vertical driver system for which the velocity transducer was mounted on top of the cryostat. For recording the 4.2 K spectra the inner chamber of the cryostat was flooded with liquid helium. The variable-temperature spectra were recorded in a flow of helium gas that was admitted in the sample space

through a capillary and was controlled using a needle valve and a Cryocon 32B temperature controller. The isomer shift values are reported relative to α-Fe at 298 K. The spectra were analyzed within the framework of a two-spin Hamiltonian as implemented by the 2spin option of the WMoss software (SeeCo, formerly Web research Co., Edina, MN).

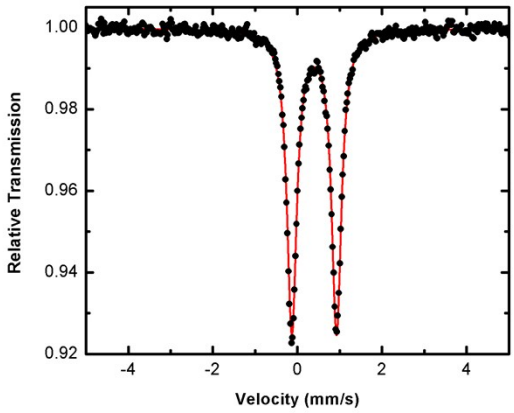

Figure S9. 80 K ^{57}Fe Mössbauer spectrum of **Fe(Py$_2$TTA)Cl$_2$** with fit (red line) corresponding to δ = 0.40 mm/s, ΔE_Q = 1.06 mm/s.

At 4.2 K the 0.0 T spectrum exhibits a six-line hyperfine splitting pattern that spans more than 10 mm/s and is indicative for the presence of sizable magnetic field acting on the ^{57}Fe nuclei. Although for Kramers systems such as Fe^{III} ions with S = 5/2 ground spin states, the existence of a spontaneous magnetic hyperfine structure at low temperature is expected,[3] analysis of the 4.2 K spectra suggests that the observed hyperfine splitting pattern is a manifestation of a magnetically ordered state, see Figure S10. Increasing the temperature from 4.2 to 15 K leads to a dramatic change in the hyperfine splitting pattern from a sextet to a two line pattern (i.e., quadrupole doublets, see Figure S11).

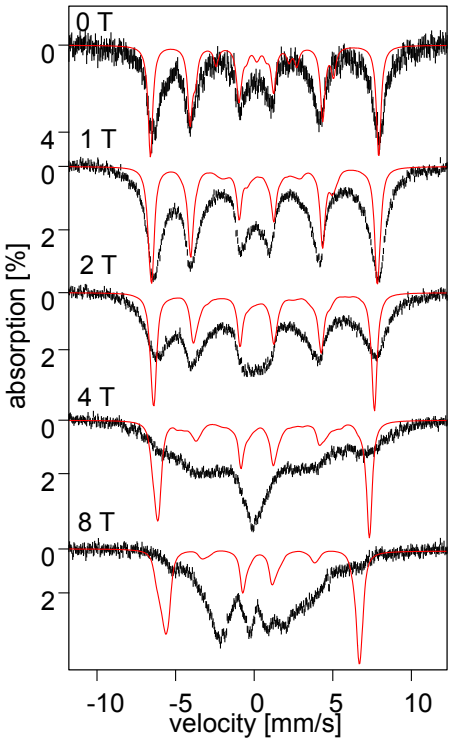

Figure S10. Variable - field ^{57}Fe Mössbauer spectra recorded at 4.2 K for **1**. The solid red lines are simulations obtained for a single $S = 5/2$ spin system using a standard Hamiltonian, assuming a slow relaxation regime, and $\delta = 0.4$ mm/s, $\Delta E_Q = 1.05$ mm/s, $\eta = 1$, $D = -1$ cm^{-1}, $E/D = 0.0$, $g_x = g_y = g_z = 2.0$, $A_x = A_y = -19.0$ T, $A_z = -18.0$ T. The D, E/D and g values were chosen such that they are representative of typical high-spin Fe^{III} sites. The A values were selected such that the predicted splitting matches that observed experimentally in zero-field. δ and ΔE_Q were determined from the high-temperature spectra. These simulations are presented in order to illustrate the dramatic difference between the hyperfine splitting pattern expected for a typical h.s. Fe^{III} ion and that observed experimentally. We note that unlike this model, the Hamiltonian described by equations 1a-c and the parameters of Table 2, in zero-field predict a null magnetic hyperfine splitting regardless of the relaxation regime and temperature.

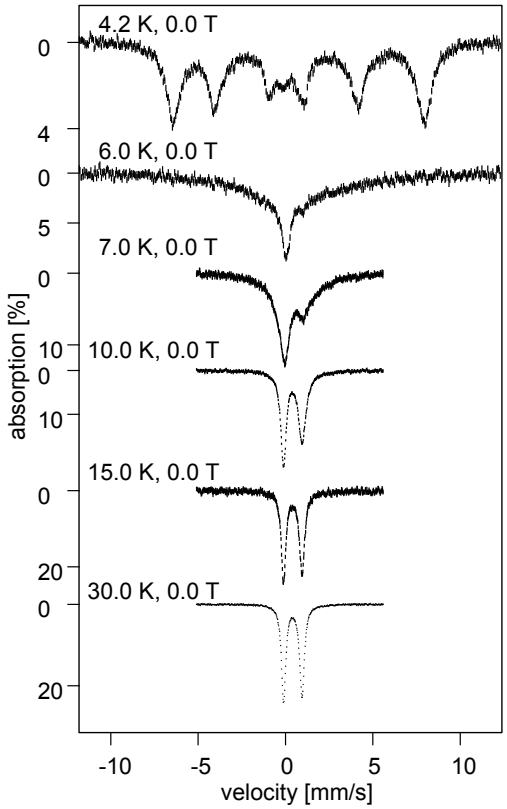

Figure S11. Zero-field Mössbauer spectra recorded for a ground solid sample of **1**. Inspection of these spectra shows that while the 4.2 K spectrum is dominated by the magnetic hyperfine splitting spectra recorded above 15 K consist of just a quadrupole doublet.

This finding suggests that while at 4.2 K the electronic spin is in a slow relaxation regime, with a spin flip rate smaller than 10^5 s^{-1}, the increase in temperature results in an increase in the spin-flip rate, presumably due to a transition from an ordered state to a paramagnetic phase. Thus, at 15 K the magnetic hyperfine splitting observed at lower temperatures is fully collapsed demonstrating that the non-zero magnetic hyperfine interactions are averaged out due to the fast relaxation of the electronic spins.[4] These observations indicate that, above 10 K, the field - dependent spectra can be analyzed within the framework of a spin-Hamiltonian model by assuming a fast relaxation regime, i.e., a spin flip rate higher than 10^{-7} s^{-1}. Figure 8 shows a series of selected field dependent spectra recorded at 15 K and variable-temperature spectra obtained in an applied field of 8 T. These spectra have been analyzed within the framework of a two S = 5/2 spin model for which the two local sites were kept identical and the spin coupling exchange constant considered was isotropic (see Eq. 1a-c). The choice of the local spin values is

justified both by the analysis of the magnetic susceptibility data, in particular by the value of the Curie constant determined from the slope of the $1/\chi$ *vs*. *T* trace, and by the values of the zero-field Mössbauer parameters. The need for including exchange interactions is not only demonstrated by the low temperature magnetic behavior but also warranted by the presence in the solid state of strong intermolecular interactions between near neighbors, *vide supra.*

For temperatures such that kT >> $D_{1,2}$ ~ J_{12} we expect a Curie-type behavior, that is $\langle \hat{S} \rangle_{th} \sim 1/T$. Consequently, under these conditions the magnetic hyperfine splitting is nearly independent of the local ZFS and of the intermolecular exchange interactions. The simulations of the high temperature spectra yield a $B_{effective}$ = 3.9 (*4.4*) T at 150 (*180*) K. Considering that for a *S* = 5/2 with null ZFS $\langle \hat{S}_{x,y,z} \rangle_{th}$ = -0.21(0.17), these $B_{effective}$ values yield a hyperfine coupling tensor such that the isotropic component A_{iso} = -20(25) T. This A_{iso} value is in the range expected for high-spin ferric ions and is thus consistent with the zero-field Mössbauer parameters. Whereas the field-dependent, high-temperature spectra can be well understood within the framework of an *S* = 5/2 spin-Hamiltonian, inspection of Figure S12a shows that as the temperature is lowered an increasing discrepancy develops between the experimental hyperfine splitting (shown by the blue dots) and that expected for an isolated *S* = 5/2 spin obtained for an A_{iso} = -21.5 T (blue dotted trace). Moreover, at 15 K regardless of the applied field value the observed magnetic hyperfine splitting is essentially half of that expected for a typical mononuclear Fe^{III} site, see Figure S12b. In order to rationalize this discrepancy we took into consideration the effect that small exchange interactions between near molecular neighbors have on the predicted spectroscopic behavior of **1**. Thus, we found that at 15 K, for 3 cm^{-1} > J > 0 cm^{-1}, the magnitude of the hyperfine splitting is essentially inversely proportional to J that is, $\langle \hat{S}_{x,y,z}(k = 1,2) \rangle_{th} \sim 1/J$ (see Figure S13). Since $\vec{B}_{internal} \approx \langle \hat{S} \rangle_{th} \tilde{A}$ the magnetic hyperfine splitting of the 15 K spectra can be equally well reproduced by trading J for A that is, an increase in J leads to a decrease in the apparent A values. This observation is illustrated by Figure S12c which shows that the A values derived from the simulations of the 15 K spectra for fixed J (blue dots) exhibit a quadratic dependence on J (purple trace). Although this quadratic dependence leads to an infinite manifold of A tensors and J values the hyperfine splitting pattern of the variable-temperature spectra could be reproduced only by considering J = 2.7(4) cm^{-1} and A_{iso} = -21(1) T. Finally, our initial simulations suggested that at 130 - 180 K the largest component of the hyperfine coupling tensor

is aligned with the smallest component of the EFG tensor. However, at 15 K the smallest component of the EFG tensor is aligned with the smallest component of the hyperfine coupling tensor **A**. Since the effects of the ZFS are felt only at low temperatures this incongruity is resolved by introducing a small ZFS tensor that is axial, characterized by a positive D value, and which is oriented such that its largest component is aligned with the large negative component of the EFG tensor and the smallest component of the hyperfine coupling tensor **A** (see Table 2).

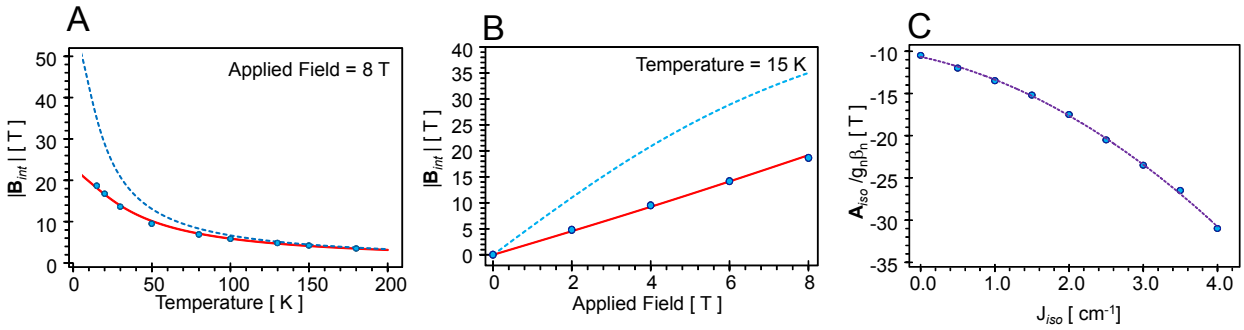

Figure S12. (a, b) Experimental (blue dots) and predicted (solid red lines obtained using equations 1a-c and the parameters of Table 2 and dotted blue lines predicted for an isolated S = 5/2 site) internal fields derived from the analysis of the temperature-dependent spectra recorded in 8 T (a) and variable-field spectra recorded at 15 K (b). (c) A *vs*. J dependence derived from the simulations of 15 K spectra.

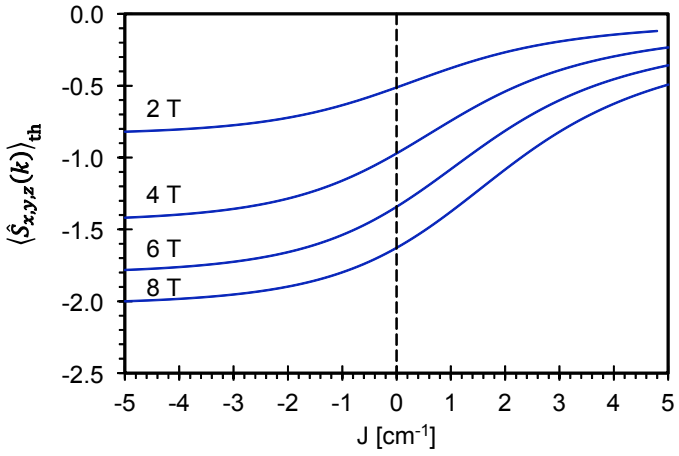

Figure S13. Thermally averaged spin expectation values $\langle \hat{S}_{x,y,z}(k=1,2)\rangle_{th}$ obtained using equation 1a calculated at 15 K and the fields listed in the figure. For clarity we have omitted the ZFS that is, we have set $D_{1,2}$ =0.0 cm^{-1}.

Computational Methodology. Density Functional Theory (DFT) calculations have been performed using the *Gaussian 09* program. The spin-unrestricted method was employed. Wave function stability calculations were performed to confirm that the calculated wave functions corresponded to the electronic ground state. The structure of the **Fe(Py_2TTA)Cl_2** complex was optimized at the spin-unrestricted PBEPBE/TZVP (with the empirical Grimme's DG3 dispersion correction) and B3LYP/6-311G levels of theory using the X-ray structure and respectively, a structural model built from scratch as the initial points. For both models the geometry optimization obtained using a spin of 5/2 in the gas phase resulted in an energy minimum with C_{2V} symmetry and with a close resemblance to the X-ray structure. Tight SCF convergence criteria (10^{-8} a.u.) were used for all calculations. Harmonic frequency calculations with the analytic evaluation of force constants were used to determine the nature of the stationary points. The molecular orbitals of the complex were calculated at the same level of theory as the optimization but adding the implicit solvent model (SMD) with CH_2Cl_2 as a solvent.

The spin density distribution for this electronic state is shown in Figure S14. The MPA-derived spin densities for Fe and Cl atoms and the L ligand are 3.93, 0.28 and 0.51 a.u. The N and S atoms of the ligand carry a spin density in the 0.06-0.14 a.u. range. The NPA-derived spin densities have similar values (3.77 for Fe, 0.30 for each Cl, and 0.62 for the tridentate ligand). The NPA charge of the tridentate ligand is -0.027 a.u. Such charge and spin density distributions imply that the valence description of the ground electronic states of the complex is between Fe^{II}-L^0, with a radical on the neutral tridentate ligand, and Fe^{III}-L^{-1}, with the closed-shell description of the anionic tridentate ligand. This "mixed" valence nature of the complex may explain the unusual spectroscopic parameters recorded for the complex. The predicted isomer shift was determined for the B3LYP/6-311G optimized structure using the calibration given by Vrajamasu et al.[8] The electric field gradient parameters, ΔE_Q and η, were obtained using the *efg* option of the *prop* Gaussian keyword. The initial guess of the broken-symmetry calculations were obtained using the *fragment* option of the *guess* keyword. The J_{ij} values were obtained using the expression $J = \frac{2}{25}(E_F - E_{BS})$ where the E_{BS} and E_F energies were obtained from single-point calculations.

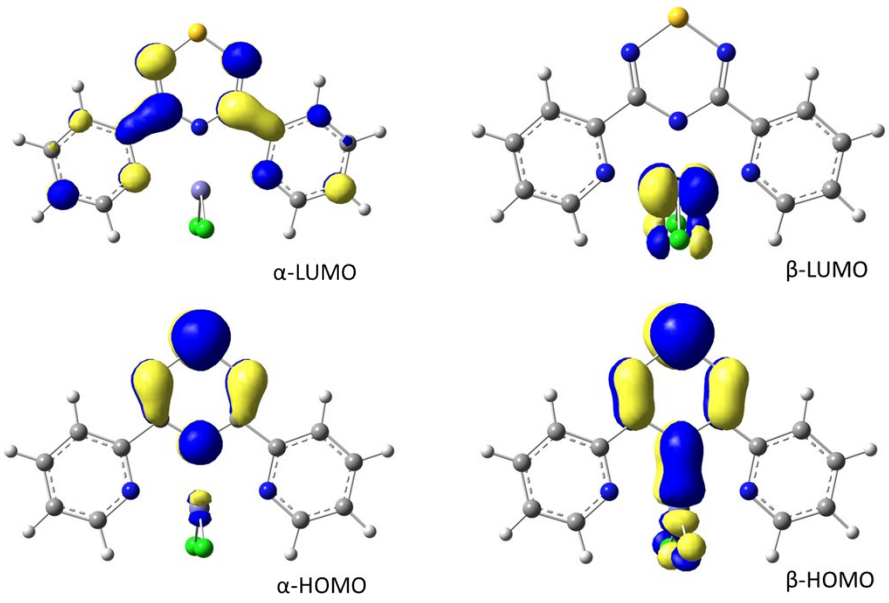

Figure S14. Frontier spin orbitals of the **Fe(Py_2TTA)Cl_2** complex (shown with the isosurface values of 0.05).

Table S3. Cartesian coordinates of the optimized structure obtained and the total SCF energy obtained using the PBEPBE/TZVP functional/basis set combination.

Fe	0.000000	0.000000	1.151083
Cl	1.884690	0.000000	2.341055
Cl	-1.884690	0.000000	2.341055
S	0.000000	0.000000	-3.881965
N	0.000000	0.000000	-0.876786
N	0.000000	1.387187	-2.866907
N	0.000000	-1.387187	-2.866907
N	0.000000	2.103953	0.620318
N	0.000000	-2.103953	0.620318
C	0.000000	1.194576	-1.581647
C	0.000000	-1.194576	-1.581647
C	0.000000	2.383767	-0.701064
C	0.000000	3.699854	-1.176746
H	0.000000	3.869822	-2.253200
C	0.000000	4.740109	-0.253013
H	0.000000	5.777165	-0.592636
C	0.000000	4.442451	1.116434
H	0.000000	5.231540	1.868521
C	0.000000	3.109068	1.513141
H	0.000000	2.812277	2.563268
C	0.000000	-2.383767	-0.701064
C	0.000000	-3.699854	-1.176746
H	0.000000	-3.869822	-2.253200
C	0.000000	-4.740109	-0.253013
H	0.000000	-5.777165	-0.592636
C	0.000000	-4.442451	1.116434
H	0.000000	-5.231540	1.868521

C	0.000000	-3.109068	1.513141
H	0.000000	-2.812277	2.563268

E(SCF)= -3316.952917 a.u.

Table S4. Cartesian coordinates of the optimized structure obtained and the total SCF energy obtained using the B3LYP/6-311G functional/basis set combination.

Fe	0.000535	0.000000	0.000000
Cl	-0.000399	1.265866	1.902350
Cl	-0.000399	1.265866	-1.902350
S	-0.000399	-5.083175	0.000000
N	-0.000032	-1.991208	0.000000
N	-1.452292	-3.956829	0.000000
N	1.451615	-3.957283	0.000000
N	-2.087610	-0.449396	0.000000
N	2.088005	-0.450051	0.000000
C	-1.214978	-2.679960	0.000000
C	1.214754	-2.680339	0.000000
C	-2.387358	-1.774012	0.000000
C	-3.709366	-2.218945	0.000000
H	-3.900257	-3.280517	0.000000
C	-4.732665	-1.274284	0.000000
H	-5.765286	-1.593343	0.000000
C	-4.415497	0.089151	0.000000
H	-5.188187	0.842815	0.000000
C	-3.079516	0.470586	0.000000
H	-2.774406	1.505164	0.000000
C	2.387395	-1.774784	0.000000
C	3.709278	-2.220034	0.000000
H	3.899907	-3.281651	0.000000
C	4.732839	-1.275655	0.000000
H	5.765357	-1.595012	0.000000
C	4.416048	0.087878	0.000000
H	5.188958	0.841320	0.000000
C	3.080198	0.469679	0.000000
H	2.775389	1.504353	0.000000

E(SCF) = -3318.25586615 Hartrees

Figure S15 depicts a unit cell projection where the molecule in grey was utilized as the point reference. A small yet non-negligible exchange interaction of $J = 0.31$ cm^{-1} was found between molecules where a number of short contacts between the TTA rings exist (e.g., grey and red molecules in Figure S15). The relatively small coupling constant observed is not surprising due to the weak nature of intermolecular radical-radical interactions (Figure 6b, c). These results are expected as the spin density primarily exists on the central TTA ring and the coordinated iron atom, with little to no spin density on the pyridyl substituents (see main text). Even smaller coupling constants were observed for the interactions between the grey molecule with others in the unit cell (e.g., blue and green) such that those J values are 1-3 orders of magnitude smaller.

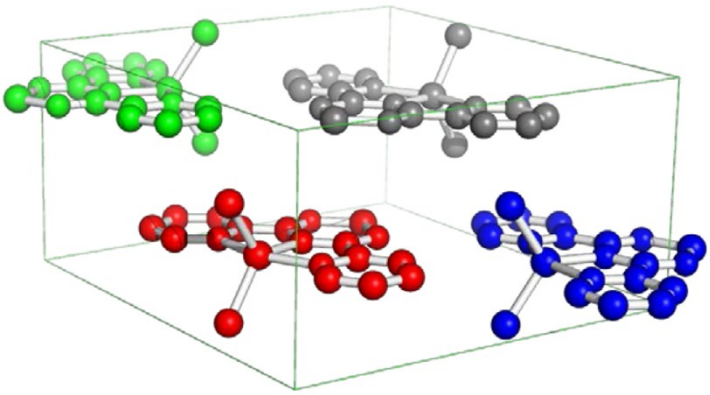

Figure S15. Schematic representation of the unit cell, highlighting the relative orientations of the four distinct molecules comprising the unit cell. Molecule shown in grey used as point reference. Exchange coupling constants between this molecule and red J = 0.31 cm^{-1}, blue J = 0.05 cm^{-1}, and green J = 0.0007 cm^{-1}.

References

1. Leitch, A. A.; Korobkov, I.; Assoud, A.; Brusso, J. L., *Chemical communications (Cambridge, England)* **2014,** *50* (38), 4934-6.
2. Boere, R. T.; Moock, K. H.; Parvez, M., *Zeitschrift Fur Anorganische Und Allgemeine Chemie* **1994,** *620* (9), 1589-1598.
3. Que, L. J. e., In *Physical Methods in Bioinorganic Chemistry*, University Science Books: Sausalito, California, 2000.
4. Abragam, A.; Bleaney, B., *Electron Paramagnetic Resonance of Transition Ions*. Clanderon: Oxford, 1970; Bhargava, S. C.; Knudsen, J. E.; Morup, S., *Journal of Physics C-Solid State Physics* **1979,** *12* (14), 2879-2896.
5. APEX Software Suite v.2012, A. S. S.; Bruker AXS: Madison, WI., **2005**.
6. Blessing, R. H., *Acta Crystallographica Section A* **1995,** *51*, 33-38.
7. Sheldrick, G. M., *Acta Crystallographica Section A* **2008,** *64*, 112-122.
8. Vrajmasu, V.; Munck, E.; Bominaar, E. L., *Inorganic Chemistry* **2003,** *42* (19), 5974-5988.